Available online at www.sciencedirect.com
ScienceDirect
Journal of Power Sources 179 (2008) 754–762
JOURNAL OF POWER SOURCES
www.elsevier.com/locate/jpowsour

High-throughput studies of $Li_{1-x}Mg_{x/2}FePO_4$ and $LiFe_{1-y}Mg_yPO_4$ and the effect of carbon coating

Matthew R. Roberts [a], Girts Vitins [b], John R. Owen [a,*]

[a] *School of Chemistry, University of Southampton, Southampton, SO17 1BJ, UK*
[b] *Now at QinetiQ, Haslar Road, Gosport, PO12 2AG, UK*

Received 25 September 2007; received in revised form 3 December 2007; accepted 10 January 2008
Available online 30 January 2008

Abstract

A two-dimensional sample array synthesis has been used to screen carbon-coated $Li_{(1-x)}Mg_{x/2}FePO_4$ and $LiFe_{(1-y)}Mg_yPO_4$ powders as potential positive electrode materials in lithium ion batteries with respect to x, y and carbon content. The synthesis route, using sucrose as a carbon source as well as a viscosity-enhancing additive, allowed introduction of the Mg dopant from solution into the sol–gel pyrolysis precursor. High-throughput XRD and cyclic voltammetry confirmed the formation of the olivine phase and percolation of the electronic conduction path at sucrose to phosphate ratios between 0.15 and 0.20. Measurements of the charge passed per discharge cycle showed that the capacity deteriorated on increasing magnesium in $Li_{(1-x)}Mg_{x/2}FePO_4$, but improved with increasing magnesium in $LiFe_{(1-y)}$ Mg_yPO_4, especially at high scan rates. Rietveld-refined XRD results on samples of $LiFe_{(1-y)}Mg_yPO_4$ prepared by a solid-state route showed a single phase up to $y = 0.1$ according to progressive increases in unit cell volume with increases in y. Carbon-free samples of the same materials showed conductivity increases from 10^{-10} to 10^{-8} S cm^{-1} and a decrease of activation energy from 0.62 to 0.51 eV. Galvanostatic cycling showed near theoretical capacity for $y = 0.1$ compared with only 80% capacity for undoped material under the same conditions.

Keywords: $LiFePO_4$; Lithium battery; Mg doping; High-throughput; Conductivity; Carbon coating

1. Introduction

LiFePO4 is of great interest as a safe, environmentally acceptable positive electrode for lithium ion batteries [1,2], but suffers from a low intrinsic electronic conductivity. Several authors have successfully introduced a surface coating of pyrolytic carbon from sucrose [3] and other precursors [4–6] after synthesis as a means of enhancing the surface conductivity, and therefore the rate performance. Recent work in our laboratory focused on a one-step synthesis method which includes sucrose in a pyrolytic sol–gel synthesis of $LiFePO_4$ from a mixed salt solution precursor [7]. In this work sucrose also acted as a viscosity-enhancing additive to suppress individual crystal growth of precursor components during the initial drying process. The resulting uniformity of the elemental distribution is an advantage in the synthesis of doped materials by introducing a soluble form of the dopant into the precursor.

Several papers have suggested metal ion doping as a method for improving performance [8–10]. Substituting Mg and other species on the Li site was reported by Chung et al. [8] to give a $\sim 10^8$ fold increase in conductivity of $LiFePO_4$ and a greatly improved electrode performance. However, the interpretation of these results was questioned by Ravet et al. [11] who suggested that the improved conductivity may be a result of carbon residues rather than the effect of the dopant ion. To the best of our knowledge further investigation into the substitution of Li by Mg has been limited to just two further publications [12,13], which also report improved conductivity and performance.

The first reported work on $LiFe_{1-y}Mg_yPO_4$ materials was presented by Barker et al. [14] who successfully synthesized $LiFe_{0.9}Mg_{0.1}PO_4$ via a carbothermal reaction and reported "outstanding ionic reversibility". Later several publications confirmed the formation of this material under different synthesis conditions and reported improved capacity, conductivity and rate capability [15–19]. The explanation for these improvements var-

* Corresponding author. Tel.: +44 2380 592184; fax: +44 2380 593781.
E-mail address: jro@soton.ac.uk (J.R. Owen).

0378-7753/$ – see front matter © 2008 Elsevier B.V. All rights reserved.
doi:10.1016/j.jpowsour.2008.01.034

ied between an increased conductivity (ionic and electronic) in the carbon-free material and the presence of carbon due to the pyrolysis of organic material.

The above background suggests that there is a general interest in the effects of Mg as a dopant in $LiFePO_4$ and particularly a need for more data concerning the solid solution ranges and any data that may ascertain whether electrode improvements are truly due to the dopant itself or to carbon associated with the preparation method used to introduce Mg. The large number of experiments required calls for a high-throughput technique.

Recently, a number of high-throughput, or combinatorial, methods have been described for the rapid discovery of new electrode materials. For example, Dahn's group have used physical vapour deposition to fabricate composition spreads of new negative electrodes with enhanced capacity for lithium storage, e.g. Si–Al–Mn [20]. Our work has focused on arrays of positive electrode materials, using sol–gel ceramic processing methods. The post-synthesis array transfer (PoSAT) technique [21] was recently described as a rapid way of finding the optimum amount sucrose for the above sol–gel synthesis. Here we report results from a two-dimensional array, in which the concentrations of sucrose and a dopant were varied independently. The aims of the work were:

(1) To demonstrate the application of the PoSAT high-throughput method to the fabrication of arrays of $Li_{1-x}Mg_{x/2}FePO_4$ and $LiFe_{1-y}Mg_yPO_4$ electrode samples prepared under identical conditions except for variations in x, y and the amount of carbon precursor.
(2) To demonstrate a high-throughput screening technique to detect any significant correlations between the rate performance and magnesium doping of samples where the electronic conductance path to the active material is optimised.
(3) To confirm any trends found in the high-throughput screening experiment by conventional methods.

2. Experimental

2.1. Electrode array preparation by post-synthesis array transfer (PoSAT)

Four 250 mL aqueous solutions A, B, C and D were prepared with the chemical compositions reported in Table 1. Appropriate aliquots of each solution were dispensed into 64 quartz microtubes (2 mL capacity) using hand-automated pipettes (Finnpipette adjustable-volume digital pipettes) so that the first four rows top to bottom on the array had increasing values of x in $Li_{1-x}Mg_{x/2}FePO_4$ ($x = 0$, 0.02, 0.04 and 0.06) and the bottom four rows y increased in $LiFe_{1-y}Mg_yPO_4$ ($y = 0.05$, 0.1, 0.15 and 0.2). (These compositions are shown in Table 2 along with the specific capacity for each assuming the Mg is inactive. The range of compositions was chosen to reflect the dopant levels reported in the literature cited in this work.) Also in the columns of the array from left to right the ratio of sucrose to phosphoric acid was increased (0.05, 0.1, 0.15, 0.2, 0.22, 0.25 and 0.30). (In this case, the sucrose to phosphoric acid (instead of iron) ratio (SPR) will be used to define the amount of sucrose across an array of different iron contents.) These solutions were then agitated using a Fischer "Whirlimix" Vortex mixer to ensure homogeneity before being placed in an oven at 70 °C for 12 h to remove the water. The array of precursor solids was then calcined in an argon atmosphere at 700 °C using a large bore (80 mm diameter) tube furnace (Lenton). After cooling, the products were crushed to a powder using a glass rod attached to a drill. Composite electrode preparation began by adding two inks, 4% PVdF-HFP (Aldrich, polyvinylidene fluoride-co-hexafluoropropylene) and 4% AB (acetylene black, Shawinigan, Chevron Phillips Chemical Company LP) in cyclopentanone (CP) to the active material powders with five 1 mm zirconia beads placed in each tube. The inks were added to give a final mass ratio of 10% PVdF-HFP, 25% AB and 65% active material and then mixed using the vortex mixer. (An unusually high AB loading was chosen to eliminate the effects of resistance in the composite matrix and focus on the mass/charge transport restrictions within the active material itself.) Then 14 μL aliquots of each ink were deposited onto the appropriate position on the array of aluminium current collectors and spread across the surface to form an even film of ink. At the same time, a 40 μL sample of each ink was deposited into an array of alumina micro-crucibles for thermogravimetric analysis as detailed

Table 2
Compositions of materials prepared, the material theoretical specific capacity assuming the Mg is inactive and the location on the array

$Li_{1-x}Mg_{x/2}FePO_4$	Row 1	Row 2	Row 3	Row 4
x	0	0.02	0.04	0.06
Specific capacity (mA h g^{-1})	169.9	166.4	162.9	159.38
$LiFe_{1-y}Mg_yPO_4$	Row 5	Row 6	Row 7	Row 8
x	0.05	0.1	0.15	0.2
Specific capacity (mA h g^{-1})	163.0	156.0	148.9	141.6

Table 1
Solutions used to prepare a graded composition array

Solution	Chemical concentrations
A	0.625 M $Fe(NO_3)_3{\cdot}9H_2O$ (Avocado, 1.25 M), 0.625 M $LiCH_3COO{\cdot}2H_2O$ (Fisher, 2.5 M), 0.625 M H_3PO_4 (85 wt.% Aldrich)
B	0.625 M $Fe(NO_3)_3{\cdot}9H2O$ (Avocado, 1.25 M), 0.5875 M $LiCH_3COO{\cdot}2H_2O$ (Fisher, 2.5 M), 0.625 M H_3PO_4 (85 wt.% Aldrich), 0.01875 M $Mg(CH_3COO)_2{\cdot}4H_2O$ (Aldrich)
C	0.5 M $Fe(NO_3)_3{\cdot}9H2O$ (Avocado, 1.25 M), 0.625 M $LiCH_3COO{\cdot}2H_2O$ (Fisher, 2.5 M), 0.625 M H_3PO_4 (85 wt.% Aldrich), 0.125 M $Mg(CH_3COO)_2{\cdot}4H_2O$ (Aldrich)
D	2 M sucrose

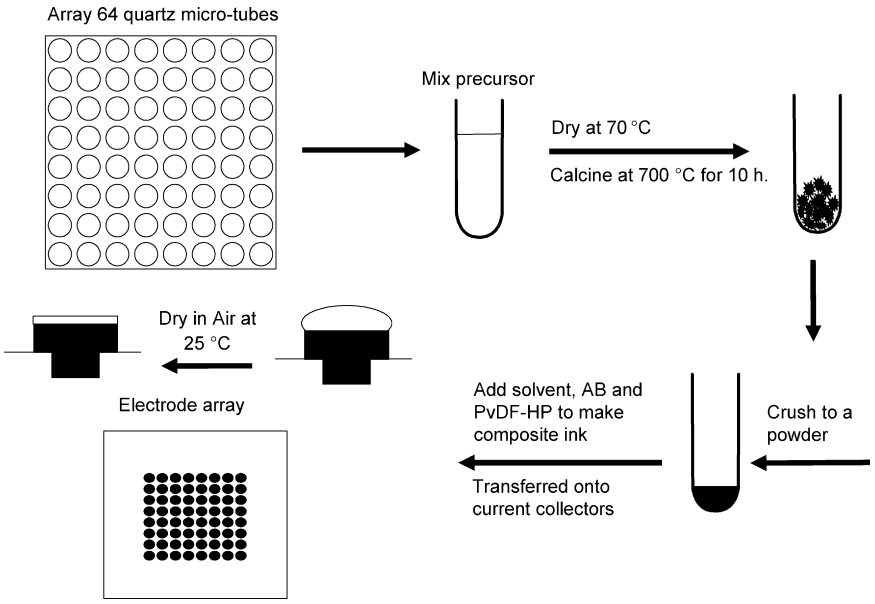

Fig. 1. Schematic diagram of the PoSAT method.

below. The CP was evaporated from both arrays at room temperature before drying at 80 °C followed by evacuation. The samples on both arrays were then accurately weighed using a computer connected balance. This preparation is depicted in Fig. 1 [21].

2.2. Determination of active masses by thermogravimetric analysis

The array of samples deposited in alumina micro-crucibles was then heated to 800 °C in air to burn off the carbon and binder. After allowing the array to cool to room temperature each sample was weighed again to measure accurately the amount of fully oxidized active material. The percentage of active material in each element of the electrode array calculated by assuming the compositions of samples were identical for corresponding positions in the two arrays.

2.3. High-throughput X-ray diffraction (HT-XRD)

For X-ray phase analysis we used a high-throughput X-ray diffractometer (Bruker AXS C2 using Cu $K\alpha_1$ radiation) which automatically records X-ray patterns of the 64 composite electrodes. The scan time was 20 min for each sample, i.e. about 24 h to record diffraction patterns across the whole array.

2.4. High-throughput electrochemical evaluation of 64 electrode arrays

The cell construction and instrumentation has been reported previously [22]. The cell consisted of a Li foil common counter/reference and a common piece of glass fibber separator soaked in 1 M $LiPF_6$ in PC. The electrode array was cycled between 2.5 and 4.5 V *vs.* Li at the following scan rates: 0.05, 0.1, 0.4, 0.8 and 1.6 mV s^{-1}.

2.5. Bulk preparation of samples $LiFePO_4$ and $LiFe_{0.9}Mg_{0.1}PO_4$

The same preparation was used as on the PoSAT array except the solution volumes were scaled up so that the total precursor volume was 20 mL. A molar ratio of 0.25 sucrose to H_3PO_4 was used in both cases.

2.6. Bulk preparation of $LiFe_{0.95}Mg_{0.05}PO_4$

$LiFe_{0.9}Mg_{0.05}PO_4$ was synthesized using a conventional, solid-state reaction. Stoichiometric amounts of Li_2CO_3 (Aldrich), $FeC_2O_4{\cdot}2H_2O$ (Aldrich), $(MgCO_3)_4{\cdot}Mg(OH)_2{\cdot}5H_2O$ (Aldrich) and aqueous solution of 85 wt.% H_3PO_4 (Aldrich) were first mixed and reacted at room temperature in a mortar until evolution of CO_2 gas ceased. The product, a yellow slurry, was transferred to an alumina boat and calcined in argon for 5 h at 700 °C. Afterward the product was ground/homogenized in the mortar and heat-treated again in flowing Ar at 700 °C for another 5 h (heating rate 25 ° min^{-1}).

2.7. X-ray phase analysis on bulk samples

X-ray powder diffraction patterns were recorded for the bulk samples using a Bruker D5000 diffractometer. X-ray patterns were collected for the 2θ between 15° and 50° at a scanning rate of ca. 0.07 ° min^{-1} using a Cu $K\alpha_1$ radiation.

2.8. Scanning electron microscopy on bulk samples

Samples of the active materials were studied by scanning electron microscopy (SEM) using a JSM6500F at an accelerating voltage between 10 and 15 kV using the secondary electron and backscattered electron detectors.

2.9. Electrochemical testing of bulk samples

Electrode films pellets containing 75 wt.% of active material, 20 wt.% of acetylene black (Shawinigan Black, 100%-compressed, Chevron AB) and 5 wt.% poly-tetrafluoroethylene (PTFE, Type: 6C-N, DuPont) binder were prepared as described previously [7]. The mass of the pellets was in the range 13–17 mg, with a thickness in the range 0.08–0.11 mm. Two-electrode cells were assembled in an argon-filled glove box (H_2O, O_2 <1 ppm; Unilab from MBraun). Lithium foil was used both as the counter and reference electrode, and 1 M $LiPF_6$ in ethylene carbonate/dimethyl carbonate (EC/DMC: 1/1 by weight, LP30, Merck) as the electrolyte soaked in two glass-fibber separators (GF/F, Whatman). Sandwiched cell materials were compressed in spring-loaded stainless steel cell holders [23]. The cells were cycled galvanostatically at a range of different currents between 2.0 and 4.5 V *vs.* Li using a 16-channel potentiostat (VMP, Princeton Applied Research; Biologic-Science Instruments).

2.10. Bulk preparations of carbon-free samples of $LiFePO_4$ and $LiFe_{0.9}Mg_{0.1}PO_4$

Carbon-free materials were synthesized using a conventional, solid-state reaction. Stoichiometric amounts of Li_2CO_3 (Aldrich), $FeC_2O_4{\cdot}2H_2O$ (Aldrich), $(MgCO_3)_4{\cdot}Mg(OH)_2{\cdot}5H_2O$ (Aldrich) and 85 wt.% H_3PO_4 (Aldrich) were first mixed to give the desired atomic ratios for $LiFePO_4$ and $LiFe_{0.9}Mg_{0.1}PO_4$. The product, a yellow slurry, was transferred to an alumina boat and calcined (10 °min^{-1}) in argon for 5 h at 700 °C under a slow flow of argon gas without rigorous air exclusion. The products, red-brown in colour indicating some oxidation, were ground in the mortar and heat-treated again in flowing 10% H_2 in Argon at 500 °C for another 3 h (heating rate 5 °min^{-1}), the lower reaction temperature being used to avoid the formation of Fe_2P). The final products were gray powders, characteristic of $LiFePO_4$.

2.11. Conductivity measurements

The pellets used for the electronic conductivity measurements were prepared by die-pressing carbon-free $LiFePO_4$ and $LiFe_{0.9}Mg_{0.1}PO_4$ powder samples (using a pressure 1.5 ton cm^{-2}) and sintering at 550 °C for 3 h in Ar. Both sides of these pellets were then coated with a Ag conductive paint (RS). The pellets had a 1.1 cm diameter and were ~0.2 cm thick. The impedance of these samples was measured between 30 and 140 °C at ~5 °C intervals using a Solartron FRA1250 frequency response analyzer with a Solartron ECI1287 electrochemical interface and a frequency range from 65 kHz to 10 Hz. Results showed a single but rather depressed semicircle in the Nyquist plot, peaking at around 100 Hz. Impedance at 10^{-3} Hz and measurement of the current response to potential steps confirmed that there was little dispersion at very low frequency. The low frequency impedance was therefore interpreted as the electronic resistance. The semicircle was broadly consistent with an electronic resistance coupled to a dielectric and leads capacitance of ca. 10 pF. The extrapolated low frequency resistance was used to determine the electronic conductivity with knowledge of the sample dimensions. A similar, or smaller ionic resistance coupled with a relatively large double layer capacitance (ca. 10 μF cm^{-2}) would result in a clear high-frequency semicircle not seen in our impedance data. A much higher ionic resistance would result in a smaller low frequency semicircle which would probably be below the detection limit. Therefore we conclude that the measured resistance was electronic in nature. This was confirmed by a dc polarisation test in which the current was found to be constant over a period of 3 h.

3. Results and discussion

3.1. High-throughput structural characterisation

High-throughput XRD patterns fell into two groups, as we reported previously for pure $LiFePO_4$, depending on whether there was sufficient sucrose or carbon present to reduce all the iron (III) to iron (II) after consuming all the nitrate. Despite the effect of a little substitution of magnesium acetate (reducing) for iron (III) nitrate (oxidizing) across the array, the threshold SPR remained between 0.15 and 0.20, consistent with the previously found value of around 0.16 sucrose:iron (III) for undoped materials. The XRD patterns selected in Fig. 2 show that reduction was complete for all samples prepared at an SPR of 0.20 and above, and that the olivine phase was pure enough for the purpose of defining the mass of active electrode material. However, the HT-XRD method did not give diffraction angles with sufficient accuracy to extract lattice parameters, and that any observed differences in the values of 2θ between the selected patterns are more likely to be due to small variations in sample height than changes in lattice parameter.

3.2. High-throughput electrochemical characterisation

On examination of the CVs shown in Fig. 3a, the currents are negligible for samples with 0, 0.05 and 0.1 SPR but begin

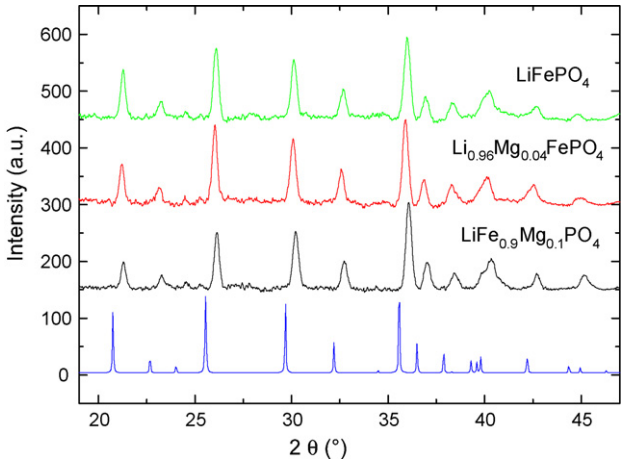

Fig. 2. Graph showing XRD patterns for array of LiFePO4 where Mg had been substituted for both Li and Fe. Shown here are patterns prepared with a SPR of 0.2. Also shown for comparison is a simulated pattern for $LiFePO_4$.

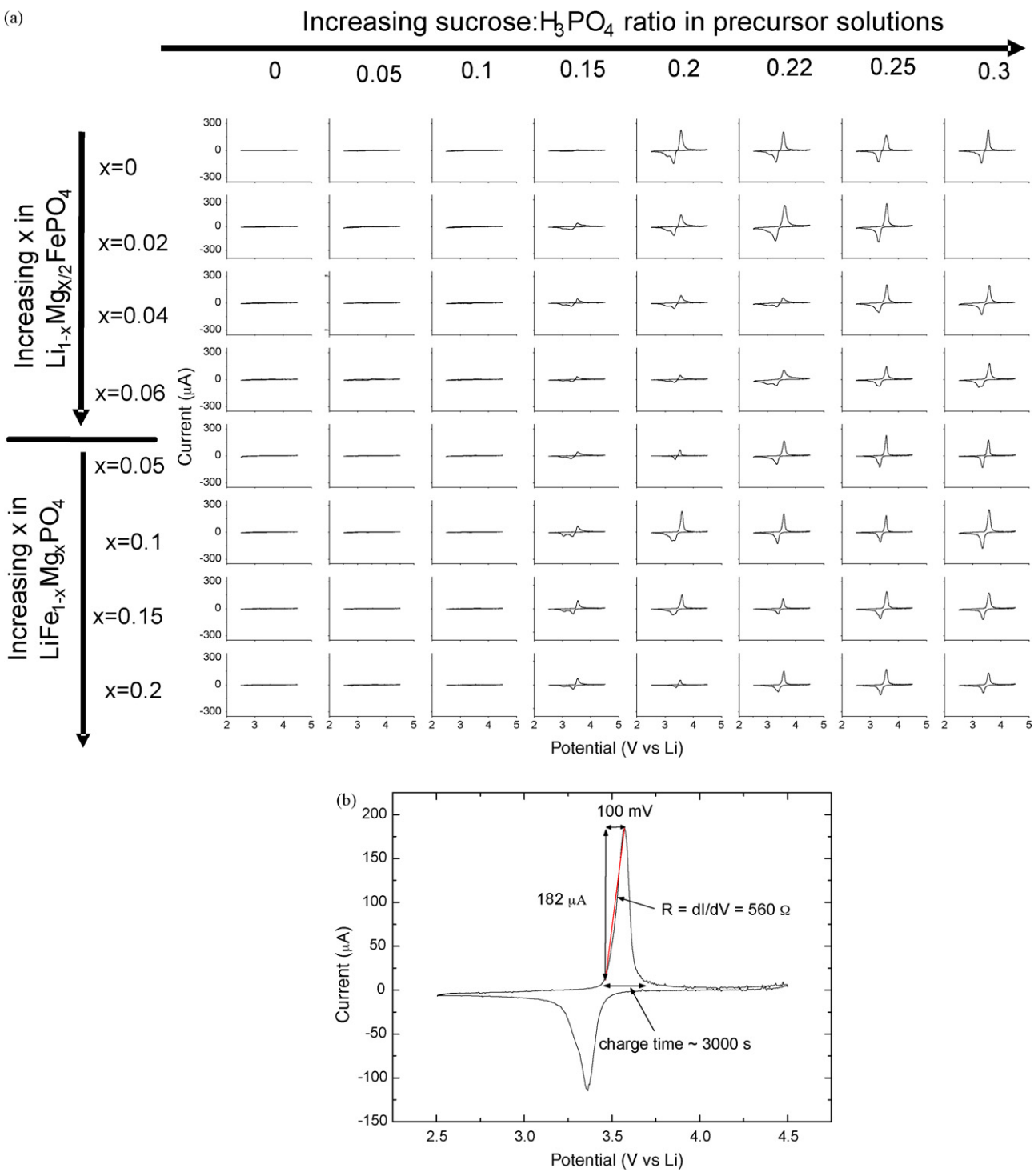

Fig. 3. (a) CVs for array of $LiFePO_4$, where Mg had been substituted for both Li and Fe. (b) Expanded example for $LiFe_{0.9}Mg_{0.1}PO_4$ prepared with a sucrose:H_3PO_4 ratio of 0.22.

to increase at 0.15 where all oxidants have been reduced and the olivine products are coated with a minimal amount of carbon. An impurity peak, occasionally seen around 2.9 V due to a Nasicon-type impurity, $Li_3Fe_2(PO_4)_3$, indicates a small inhomogeneity of the sample at this low sucrose level, which was insufficient for full reduction to iron (II). For 0.2 SPR and above and at this slow scan rate, most of the voltammogram shapes are similar; as shown in the expanded example CV (Fig. 3b) the rising transients show a resistive limitation of about 1 kΩ which is probably due to the lithium counter electrode interface with the electrolyte, while the falling transients decay after 3000 s, corresponding to ambipolar lithium diffusion out of the particles at an average rate of approximately 1 C. The different heights of the peaks are therefore mainly due to changes in the proportion of active material that is in effective contact with the carbon network.

The increases in the discharge capacity at 0.05 mV s^{-1} are expressed in Fig. 4 (substitution of lithium) and 5 (substitution of iron) as the percentage of theoretical charge capacity released during a positive potential scan up to 4.5 V and back to the zero current point. There is tentative evidence of capacity increases in both doping schemes at the 0.15 SPR. For the Fe-substituted samples this may be due to the lower nitrate levels rather than a true doping effect. The main effects of increasing amounts of carbon are seen from 0.2 to 0.3 SPR, where the formation of a percolating conductivity network becomes increasingly probable in all cases, as was observed in our previous work [21].

Close examination of Fig. 4 shows that substitution of Mg for Li in the precursor is detrimental at SPR values above 0.15, i.e. when the carbon network is fully formed, with capacities decreasing from 70% to 40% theoretical as x increases from 0 to 0.06. Such an effect is not seen for substitution of Mg for Fe in Fig. 5, where the results above 0.2 SPR are more closely grouped together with the undoped material—i.e. magnesium substitution for iron does not reduce the charge extracted per iron atom at or below C-rates of 1 h^{-1}.

Figs. 6 and 7 show the proportions of theoretical capacity obtained at higher rates. In the case of magnesium substitution for lithium, the high rate capacities decrease more quickly than for the pure material. However, the Mg for Fe-substituted samples uniformly performed better than the pure material at scan rates 0.8 mV s^{-1} and above (corresponding to C-rates up to about 5 h^{-1} based on the average currents divided by the total charges). Higher actual specific capacities values were observed for $y = 0.05$ and 0.1 at 0.8 mV s^{-1} and also $y = 0.15$ at 1.6 mV s^{-1} (~3 C) and all samples at 3.2 mV s^{-1} (~5 C). The result is, in fact, consistent with the previous publications [17–19] although it is obtained under a different condition, where the formation of an effective electronic conducting carbon network is well established in all cases.

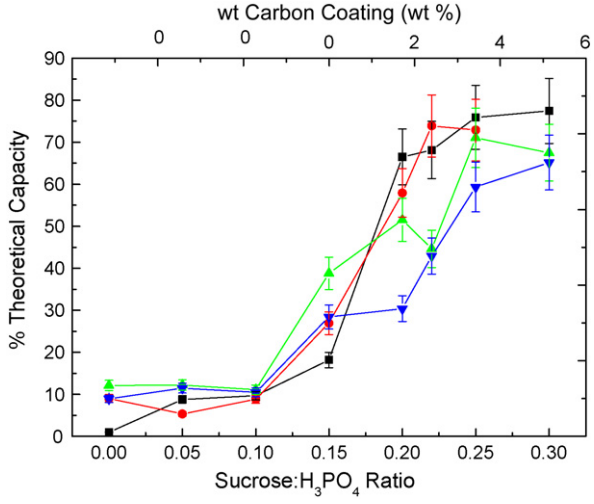

Fig. 4. Performance $Li_{1-x}Mg_{x/2}FePO_4$ ($x = 0$ (■), 0.02 (●), 0.04 (▲) and 0.06 (▼)) with various levels of sucrose during preparation (also depicted on the top x axis is the estimated wt.% carbon coating). Percentage capacities were calculated for CVs recorded at 0.05 mV s^{-1} and from the specific capacities in Table 2.

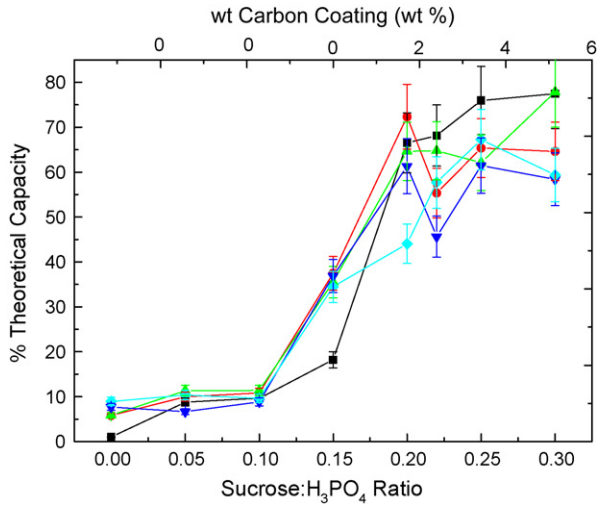

Fig. 5. Performance $LiFe_{1-y}Mg_yPO_4$ ($x = 0$(■), 0.05 (●), 0.1 (▲), 0.15 (▼) and 0.2 (♦)) with various levels of sucrose during preparation (also depicted on the top x axis is the estimated wt.% carbon coating). Specific capacities were calculated for CVs recorded a 0.05 mV s^{-1} and the specific capacities in Table 2.

To ascertain the origin of the performance improvement, we refer to the original voltammograms in Fig. 8, where the increased detail shows differences between the peak shapes for different $LiFe_{1-x}Mg_xPO_4$ samples. The effects of increasing the Mg content are as follows:

(1) increasing slopes for the rising transients during charge;
(2) increased peak height;
(3) decreased decay time constants.

The first effect is consistent with an increased electronic conductivity of the active material, under which the contact resistance with the carbon network is decreased. The second and third effects show an increased ambipolar lithium diffusion coefficient, which depends on either the ionic or the electronic conductivity, whichever is lower. Since it is less probable that

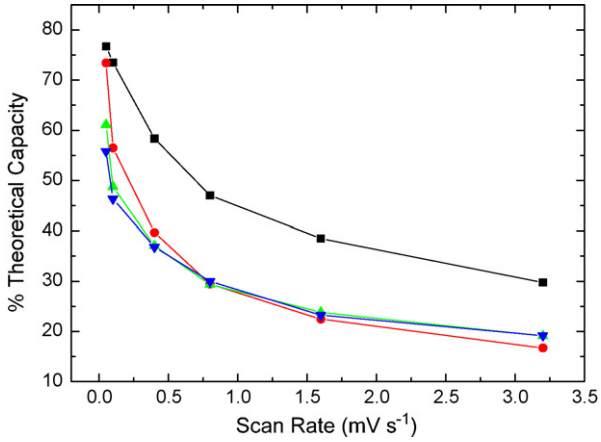

Fig. 6. Percentage of theoretical capacity obtained *vs.* scan rate for $Li_{1-y}Mg_yFePO_4$ materials where $y = 0$ (■), 0.02 (●), 0.04 (▲), 0.06 (▼). These are averaged capacity values for each material prepared with 0.22, 0.25 and 0.3 sucrose to H_3PO_4 ratio. For each x value one set of sucrose ratio capacities deviating the most from the other two was removed as an outlier.

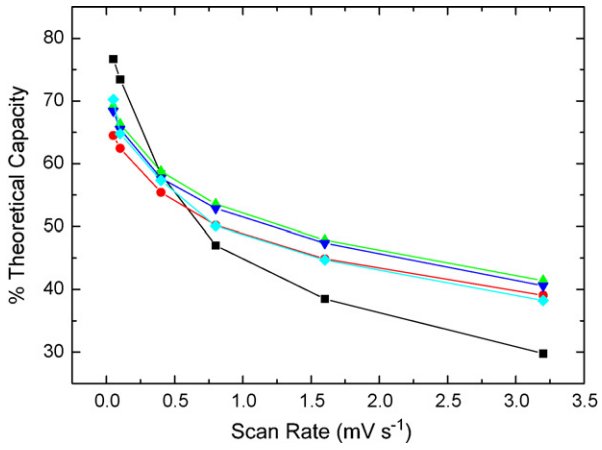

Fig. 7. Percentage of theoretical capacity obtained *vs.* scan rate for $LiFe_{1-y}Mg_yPO_4$ materials where y = 0 (■), 0.05 (●), 0.1 (▲), 0.15 (▼) and 0.2 (♦). These are averaged capacity values for each material prepared with 0.22, 0.25 and 0.3 sucrose to H_3PO_4 ratio. For each y value one set of sucrose ratio capacities deviating the most from the other two was removed as an outlier.

the substituent increases both conductivities than one, the effect is more likely to originate in the electronic conductivity.

To summarise the results of the high-throughput measurements, we report enhanced rate capability when the magnesium substituted for iron in the precursor mixture, but not when magnesium substituted for lithium. The structural analyses were not sufficiently accurate to demonstrate solid solution formation from the compositional dependence of lattice parameters.

3.3. Characterisation of $LiFe_{1-x}Mg_xPO_4$ sample from bulk preparations

Samples from bulk preparations of $LiFePO_4$, $LiFe_{0.9}Mg_{0.1}PO_4$ (prepared by the sol–gel route) and $LiFe_{0.95}Mg_{0.05}PO_4$ (prepared by solid-state reaction) were examined using the Bruker D5000 (Fig. 9). Rietveld refinement (PowderCell 2.3) based on an ordered olivine (orthorhombic) structure using space group *Pnma* gave the unit cell volumes, shown as a function of Mg substitution in Fig. 10 with a literature value for

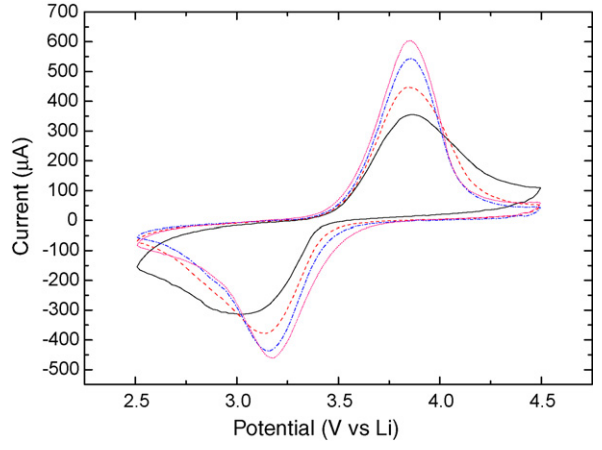

Fig. 8. CV's of $LiFe_{1-x}Mg_xPO_4$ ($x = 0$ (—), 0.05 (▬ ▬), 0.1 (▬•▬) and 0.2 (•••)) from array during cycling at 0.8 mV s^{-1}. Materials prepared with a sucrose to H_3PO_4 ratio of 0.25.

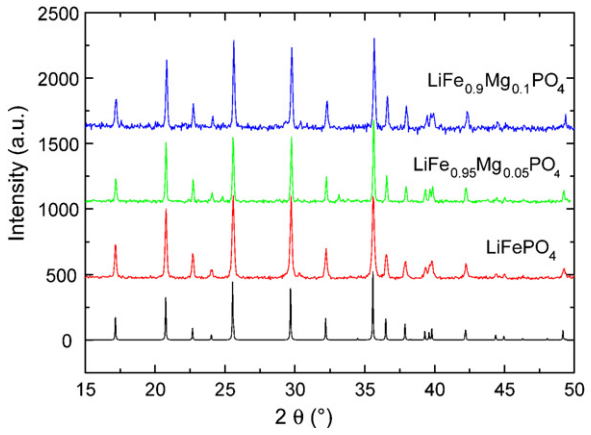

Fig. 9. XRD patterns recorded using D5000 on bulk samples.

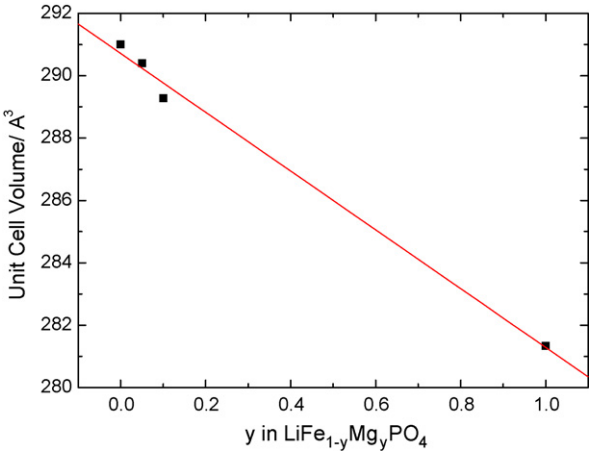

Fig. 10. Variation of unit cell volume with change *y* in $LiFe_{1-y}Mg_yPO_4$.

$LiMgPO_4$ [24] for comparison. Solid solution formation is indicated from the decrease in the unit cell volume with magnesium substitution according to Vegard's law.

For conductivity measurements, carbon-free samples of $LiFePO_4$ and $LiFe_{0.9}Mg_{0.1}PO_4$ were prepared as described above. XRD patterns showed no significant impurities. The electronic conductivity results (Table 3) indicate improvements of about 2 orders of magnitude in the measured conductivity.

The SEM images shown in Fig. 11 indicate that the $LiFe_{0.9}Mg_{0.1}PO_4$ has a similar particle size to the $LiFePO_4$, around 300–500 nm. However, the particle morphology is different; the particles in the $LiFe_{0.9}Mg_{0.1}PO_4$ are more dispersed and not held together in a large agglomerate, also the particles appear to be flatter than those in the $LiFePO_4$, presumably because of a habit modification due to the Mg.

Therefore, contributions to improved properties from morphological effects cannot be ruled out, because the large

Table 3
Conductivities of carbon-free samples of $LiFePO_4$ and $LiFe_{0.9}Mg_{0.1}PO$

	$LiFePO_4$	$LiFe_{0.9}Mg_{0.1}PO_4$
σ (S cm^{-1})	1×10^{-10}	1.4×10^{-08}
Ea (eV)	0.62 ± 0.03	0.51 ± 0.01

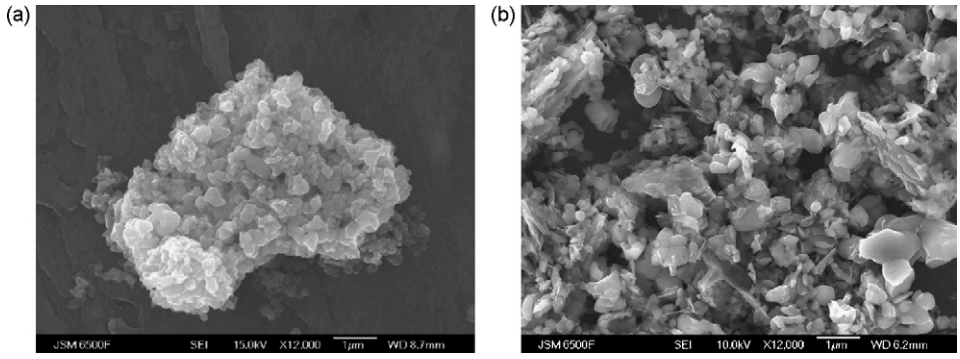

Fig. 11. SEM images of $LiFePO_4$ and $LiFe_{0.9}Mg_{0.1}PO_4$ prepared by 700 °C heat-treatment of a solution containing $LiCH_3COO$, $Mg(CH_3COO)_2$, $Fe(NO_3)_3$, H_3PO_4, and sucrose.

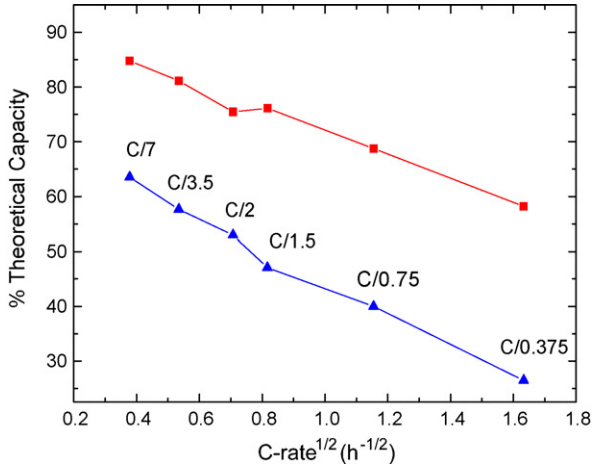

Fig. 12. Specific capacity for $LiFePO_4$ (-▲-) and $LiFe_{0.9}Mg_{0.1}PO_4$ (-■-) (both prepared via sol–gel method) *vs.* the square root of discharge rate. The discharge rate is expressed as the "C-rate," i.e., the ratio of discharge current to the theoretical charge capacity.

agglomerates of particles shown in Fig. 11a are absent in Fig. 11b. We suggest that both the morphological change and the electronic conductivity improvement may contribute to the improved material performance at higher rates.

Finally, Fig. 12 compares the performance of $LiFePO_4$ and $LiFe_{0.9}Mg_{0.1}PO_4$ which were prepared conventionally (using the sucrose pyrolysis method) and cycled galvanostatically, where the undoped material gave only 80% of the capacity of the doped material. There is a large improvement in performance for $LiFe_{0.9}Mg_{0.1}PO_4$ from the $LiFePO_4$ prepared using the same method at all C-rates. The low C-rate behaviour contrasts with slow scan rate results obtained in the high-throughput test and probably reflects the effects of compaction during electrode preparation on the electronic percolation.

4. Conclusions

An array of electrodes, prepared using the PoSAT method, has given a better understanding of the effect of increasing x and y in $Li_{1-x}Mg_{x/2}FePO_4$ and $LiFe_{1-y}Mg_yPO_4$ in the presence of an increasing level of carbon residue in the active materials.

No evidence of magnesium doping on the Li site was found in samples prepared with the stoichiometry $Li_{1-x}Mg_{x/2}FePO_4$. Higher amounts of sucrose to H_3PO_4 ratios were required to extract maximum capacity from these materials with increasing x. The maximum observed capacity was also significantly reduced by the increase of x, and no improvement in rate capability was observed.

Samples prepared with the stoichiometry $LiFe_{1-y}Mg_yPO_4$ showed a linear decrease in cell volume with increasing y, indicating Mg doping on the iron site. A slight decrease was observed in the amount of carbon required to achieve maximum capacity. By observing the high rate performance of materials prepared with high sucrose ratios we have shown an improvement in extractable capacity when Fe is replaced by Mg. We attribute this to an improvement in electronic conductivity within the active material particle, and a slight modification in sample morphology which reduces the build up of large agglomerates of small particles.

This work has highlighted the use of the PoSAT high-throughput method to discover improvements in material performance as a result of compositional variations. Its utility was as a screening method to highlight improvements due to Mg substitution for Fe, paving the way for conventional experiments designed to confirm and elaborate the result.

Acknowledgements

The authors are grateful for financial support (GV and MRR) from the EPSRC (GR/S27238/01 ADLiB project) and The University of Southampton Combinatorial Centre of Excellence (GR/M88365/01 JIF award).

References

[1] A.K. Padhi, K.S. Nanjundaswamy, J.B. Goodenough, J. Electrochem. Soc. 144 (1997) 1188–1194.
[2] A.K. Padhi, K.S. Nanjundaswamy, C. Masquelier, S. Okada, J.B. Goodenough, J. Electrochem. Soc. 144 (1997) 1609–1613.
[3] M. Armand, M. Gauthier, J.-F. Magnan, N. Ravet, U.S. Patent 033,360 (2004).
[4] H. Huang, S.C. Yin, L.F. Nazar, Electrochem. Solid-State Lett. 4 (2001).
[5] J.D. Wilcox, M.M. Doeff, M. Marcinek, R. Kostecki, J. Electrochem. Soc. 154 (2007) A389–A395.
[6] R. Dominko, J.M. Goupil, M. Bele, M. Gaberscek, M. Remskar, D. Hanzel, J. Jamnik, J. Electrochem. Soc. 152 (2005) A607–A610.

[7] A.D. Spong, G. Vitins, J.R. Owen, J. Electrochem. Soc. 152 (2005) A2376–A2382.
[8] S.Y. Chung, J.T. Bloking, Y.M. Chiang, Nat. Mater. 1 (2002) 123–128.
[9] H. Liu, Q. Cao, L.J. Fu, C. Li, Y.P. Wu, H.Q. Wu, Electrochem. Commun. 8 (2006) 1553–1557.
[10] M. Zhang, L.F. Jiao, H.T. Yuan, Y.M. Wang, J. Guo, M. Zhao, W. Wang, X.D. Zhou, Solid State Ionics 177 (2006) 3309–3314.
[11] N. Ravet, A. Abouimrane, M. Armand, Nat. Mater. 2 (2003) 702–1702.
[12] Z.P. Guo, H. Liu, S. Bewlay, H.K. Liu, S.X. Dou, Synth. Met. 153 (2005) 113–116.
[13] G.X. Wang, S.L. Bewlay, K. Konstantinov, H.K. Liu, S.X. Dou, J.H. Ahn, Electrochim. Acta 50 (2004) 443–447.
[14] J. Barker, M.Y. Saidi, J.L. Swoyer, Electrochem. Solid-State Lett. 6 (2003) A53–A55.
[15] J. Hong, C. Wang, U. Kasavajjula, J. Power Sources 162 (2006) 1289–1296.
[16] T.H. Teng, M.R. Yang, S.H. Wu, Y.P. Chiang, Solid State Commun. 142 (2007) 389–392.
[17] D. Wang, H. Li, S. Shi, X. Huang, L. Chen, Electrochim. Acta 50 (2005) 2955–2958.
[18] C. Wang, J. Hong, Electrochem. Solid-State Lett. 10 (2007) A65–A69.
[19] G.X. Wang, S. Bewlay, J. Yao, J.H. Ahn, S.X. Dou, H.K. Liu, Electrochem. Solid-State Lett. 7 (2004) A503–A506.
[20] M.D. Fleischauer, J.R. Dahn, J. Electrochem. Soc. 151 (2004) A1216.
[21] M.R. Roberts, A.D. Spong, G. Vitins, J.R. Owen, J. Electrochem. Soc. 154 (2007) A921–A928.
[22] A.D. Spong, G. Vitins, S. Guerin, B.E. Hayden, A.E. Russell, J.R. Owen, J. Power Sources 119–121 (2003) 778–783.
[23] T. Le Gall, K.H. Reiman, M.C. Grossel, J.R. Owen, J. Power Sources 119 (2003) 316–320.
[24] F. Hanic, M. Handlovic, K. Burdová, J. Majling, J. Chem. Crystallogr. 12 (1982) 99–127.